Electronic Supplementary Information (SI)

Ultrathin carbon layer-coated mesoporous core-shell-type $FeP/Fe_2O_3/C$ for the hydrogen evolution reaction

Alaaldin Adam,[§] María Isabel Díez-García,[‡] Joan Ramon Morante,[‡] Muhammad Ali,[§] Zijin Chen,[ƺ] Ziqi Tian,[ƺ] Mohammad Qamar[†§]*

[†]Materials Science and Engineering Department

[§]Interdisciplinary Research Center for Hydrogen Technologies and Carbon Management (IRC-HTCM)

King Fahd University of Petroleum and Minerals, Dhahran 31261, Saudi Arabia.

[‡]Catalonia Institute for Energy Research (IREC), Jardins de les Dones de Negre 1, 08930 Sant Adrià de Besós, Barcelona, Spain.

[ƺ]Ningbo Institute of Materials Technology and Engineering, Chinese Academy of Sciences, 1219 Zhongguan West Road, Ningbo 315201, Zhejiang, P. R. China.

*Corresponding Author: qamar@kfupm.edu.sa

Experimental

Materials

Iron (III) chloride hexahydrate (≥ 99%), anhydrous ethylene glycol (EG, 99.80%), Polyethylene glycol (PEG-400), hexamethylenediamine (HMDA, 98%), sodium hypophosphite (≥ 99%), and anhydrous ethanol were purchased from Sigma-Aldrich, while Nafion (5% w/w solution) was obtained from Alfa Aesar.

Synthesis of Fe_3O_4 Hollow nanospheres

Iron precursor, $FeCl_3.6H_2O$ (2.5 mmol), was dissolved in 20 ml anhydrous ethylene glycol. Poly ethylene glycol (250 mg) and hexamethylenediamine (580 mg) were added with continuous stirring for 2 h to form dark brown gel. The gel was then transferred into a Teflon-lined stainless steel autoclave and heated at different temperature (between 160 and 220 °C) and maintained for 12 h. After the reaction, the solution was allowed to cool to room temperature. The black product was collected and washed several times with absolute ethanol and finally dried overnight in a vacuum oven at 60 ^{0}C.

Synthesis of FeP/Fe_3O_4

Approximately 20 mg of the as prepared Fe_3O_4 powder was placed in a quartz boat along with sodium hypophosphite in a tube furnace. The furnace was heated up to the desired temperatures (350, 400 or 450 °C), and kept for 2 h. Before heating, the furnace was flushed with Ar for ~ 30 min to remove any oxygen content, and the reaction was carried out under continous flow of Ar. After the reaction, the black product was collected and used as electrocatalyst for the hydrogen evolution reaction (HER). For comparison, FeP nanoparticles were prepared following the synthethesis method reported elswhere.[S1]

Material Characterization

The morphology and microstructure of the materials were investigated with the aid of the field emission scanning electron microscope (FE-SEM, Tescan Lyra-3), transmission and high-resolution transmission electron microscope and selected area electron diffraction (TEM/HR-TEM, FEI Tecnai TF20) (SAED). Other techniques employed for the characterization of the samples were: X-ray diffractometry (XRD, Rigaku MiniFlex), BET surface area analyzer (Micromeritics ChemiSorb 2750) and X-ray photoelectron spectroscopy (XPS, Thermo Scientific ESCALAB 250Xi).

Electrochemical characterization

The HER performance was evaluated in a three-electrode cell connected to a potentiostat (EG&G 273A). A saturated calomel electrode ($Hg/HgCl_2$, SCE) and graphite rod were used as the reference and the counter electrode, respectively. The SCE potential reported in this work was converted and presented against reversible hydrogen electrode (RHE). The working electrode was prepared by drop-casting method. Typically, 10 mg of electrocatalyst and 37 µl of 1.66 % wt. Nafion® were suspended in 2 ml of water and isopropanol (30% V/V), and sonicated for approximately 30 min to obtain a homogeneous ink. 16 µL of the ink solution was dropped on a pre-cleaned glassy carbon electrode (GCE, 5.0 mm diameter), and the electrode was allowed to dry naturally. The deposition steps were repeated to achieve the desired catalyst loading. Measurements were carried out in H_2-saturated aqueous electrolytes unless mentioned otherwise, at a scan rate of 5 mVs^{-1}. All current densities were calculated against the geometrical area of the GCE, unless stated otherwise, and presented after i*R* correction. Electrochemical impedance spectroscopy (EIS) was recorded in 0.5 M H_2SO_4 between the frequency range of 100000 Hz and 0.01 Hz with ac amplitude of 10 mV. All the EIS data was normalized to the geometrical surface area of the working electrode.

Quantitative Analysis of Hydrogen Gas

The hydrogen gas produced during the electrocatalytic water splitting process was quantified using a gas chromatograph (GC). The GC was equipped with pulsed discharge helium ionization detector (PDHID). It was ensured that the electrochemical cell is tight enough so no gas can escape from the cell. Once the cell was prepared, nitrogen gas was introduced to eliminate any dissolved gases in the electrolyte and the gases present in the overhead space of the cell. Nitrogen gas was also used as carrier gas. A constant current density of 10 mA cm^{-2} was maintained for a period of 1 h. The GC was attached to one of the cell's connections via a tube. A pump was attached between the tubes that connect the cell and GC. The pump was set to suck gases from the headspace of the cell and inject them into the GC every 10 min for the analysis. The GC was calibrated with known concentrations of hydrogen gas in nitrogen gas mixture.

The Faradaic efficiency for H_2 evolution was determined using:

$$\text{Faradaic efficiency} = \frac{\text{Measured amount of hydrogen gas}}{\text{Calculated amount of hydrogen gas}}$$

The measured amount of hydrogen gas was obtained from GC. The calculated amount of hydrogen gas was computed based on the total charge transferred during a two-electron reduction, assuming a 100% Faradaic efficiency.

Theoretical calculations

The Vienna ab initio simulation (VASP) was employed to carry out first-principles calculations on the structural, electronic, and catalytic properties of CFeP (011) and CFeP (211) alloys using the projected-augmented wave (PAW) technique.[S2] The Perdew–Burke–Ernzerhof (PBE) correlation exchange functional was used with the generalized gradient approximation (GGA).[S3] The wave functions of the valence electrons were enlarged by utilizing a plane wave basis with a cutoff kinetic energy of 400 eV.

The lattice constant and atomic coordinates of all structures were optimized using a conjugate-gradient approach. The relaxing process persisted until the Hellmann–Feynman forces exerted on all atoms were lower than 0.01 eV/Å and the overall energy reached a value below 10^{-5} eV. The Monkhorst–Pack approach was used to sample the two-dimensional Brillouin zone with 5 × 5 × 1 k-points.[S4] To mitigate any potential interaction between periodic images, a vacuum layer with a thickness of 15 Å was introduced in the z-direction of all structures. The Grimme's DFT-D3 approach was used to account for van der Waals interactions between hydrogen and catalysts.[S5] The cohesive energy, which quantifies the energy needed to break down a CFeP structure into individual atoms, was computed by equation S1.

$$E_{coh} = \left(\sum n_i E_i - E_{CFeP}\right) \Big/ n_i \qquad \text{(eq. S1)}$$

where n_i is the number of i^{th} atom in the CFeP structure, E_{CFeP} and E_i represent the total energies of CFeP and isolated atom i, respectively.

The affinity between the carbon layer and FeP was quantified using equation S2.

$$E_B = E_{CFeP} - E_C - E_{FeP} \qquad \text{(eq. S2)}$$

where E_{CFeP}, E_C and E_{FeP} are the total energies of hybrid CFeP, C and FeP structures, respectively.

The catalytic activity of all structures was assessed using the Gibbs free energy change, which serves as a typical descriptor for the rate of the overall process. The Gibbs free energy of hydrogen on a catalyst can be represented by equation S3.

$$\Delta G_{H*} = \Delta E_H + \Delta E_{ZPE} - T\Delta S_H \qquad \text{(eq. S3)}$$

where ΔE_H is the energy difference of the adsorbed hydrogen atom on catalyst surface, clean surface and molecular hydrogen, ΔE_{ZPE} represents the zero-point energy difference between a hydrogen atom adsorbed on the surface and that in a gaseous H_2 molecule, $T\Delta S$ represents the change in entropy multiplied by the temperature, which accounts for the entropy loss due to adsorption. The term of $T\Delta S$ is roughly a constant as 0.24 eV.[S6]

Partial charges were obtained by Bader charge analysis.[S7] The differential hydrogen adsorption energy, ΔE_H, was calculated by equation S4.

$$\Delta E_H = E(FeP + nH) - E[FeP + (n-1)H] - E(H_2)/2 \qquad \text{(eq. S4)}$$

E(FeP + nH) and E[FeP + (n – 1)H] represent the total energy of the system with n and n – 1 hydrogen atoms adsorbed on the surface, respectively. $E(H_2)$ represents the energy of a hydrogen molecule.

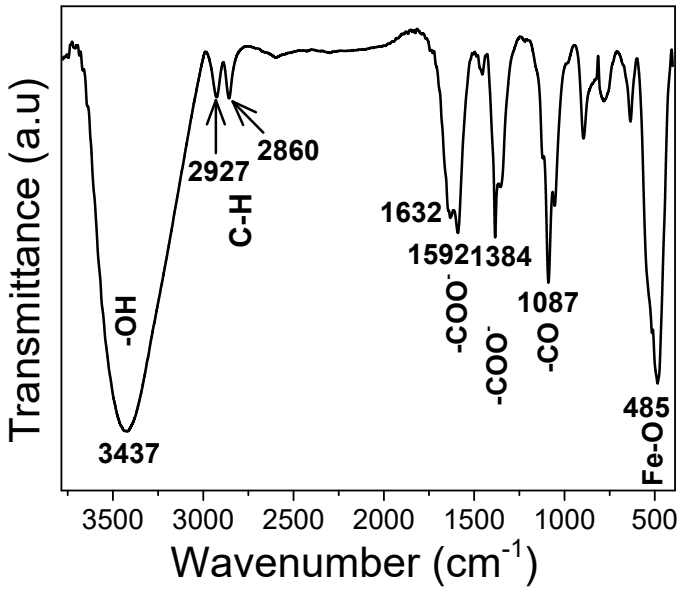

Fig. S1 FTIR spectum of iron-glycolate complex prepared at 160 °C for 12 h.

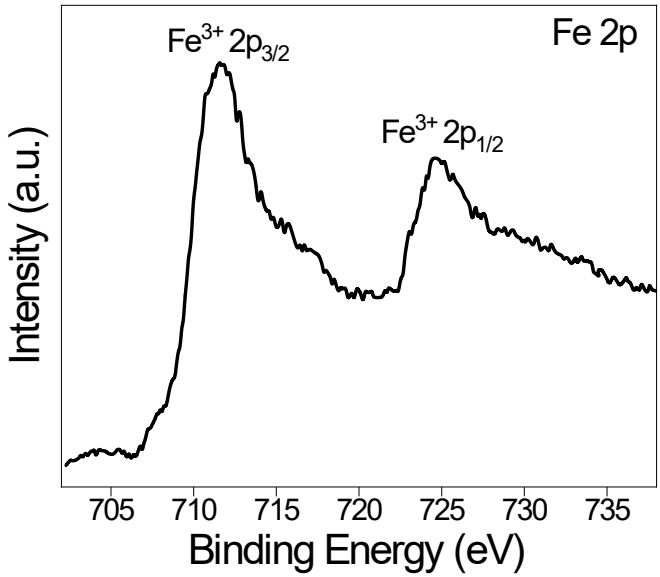

Fig. S2 XPS signatures of Fe 2p in FeP.

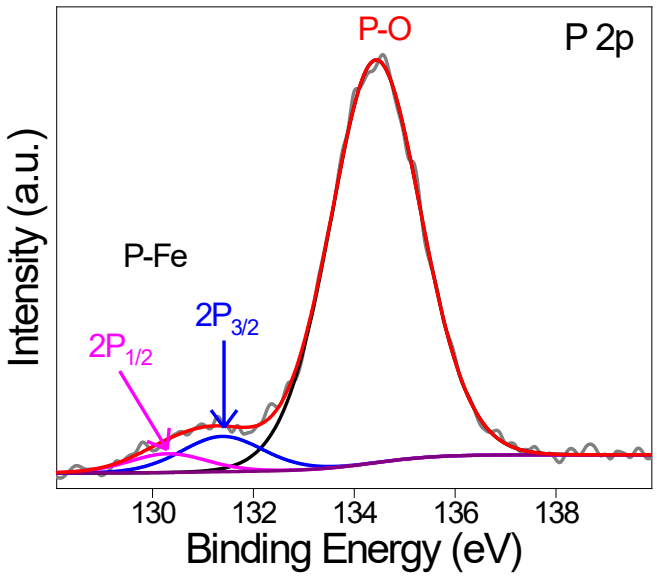

Fig. S3 XPS signatures of P 2p in FeP.

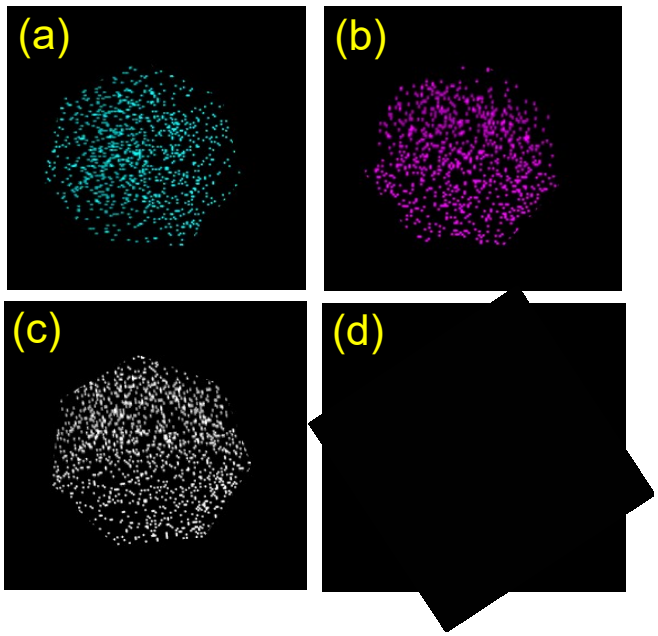

Fig. S4 Elemental mapping of the FeP/Fe_3O_4: (a) iron, (b) phosphorous, (c) carbon, and (d) = oxygen.

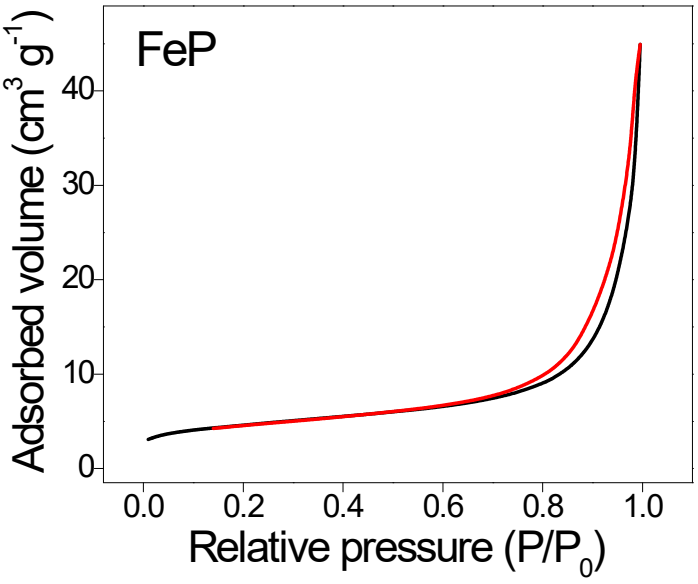

Fig. S5 N_2 adsorption-desorption isotherms of FeP.

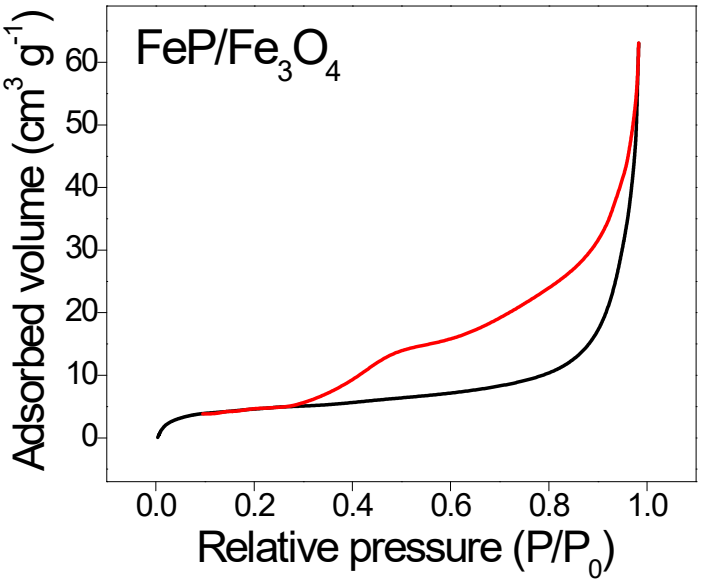

Fig. S6 N_2 adsorption-desorption isotherms of the FeP/Fe_3O_4.

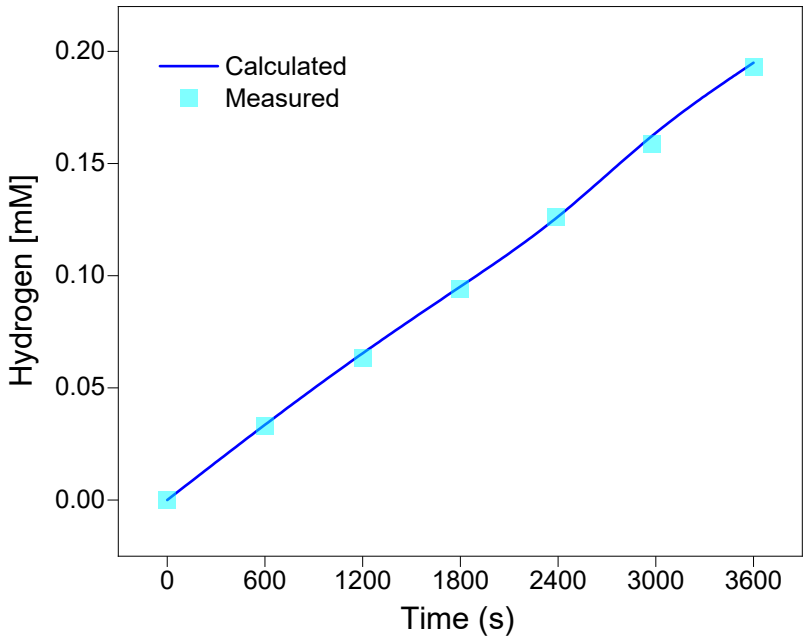

Fig. S7 Faradaic efficiency at current density of 10 mA cm^{-2}. In 0.5 M H_2SO_4.

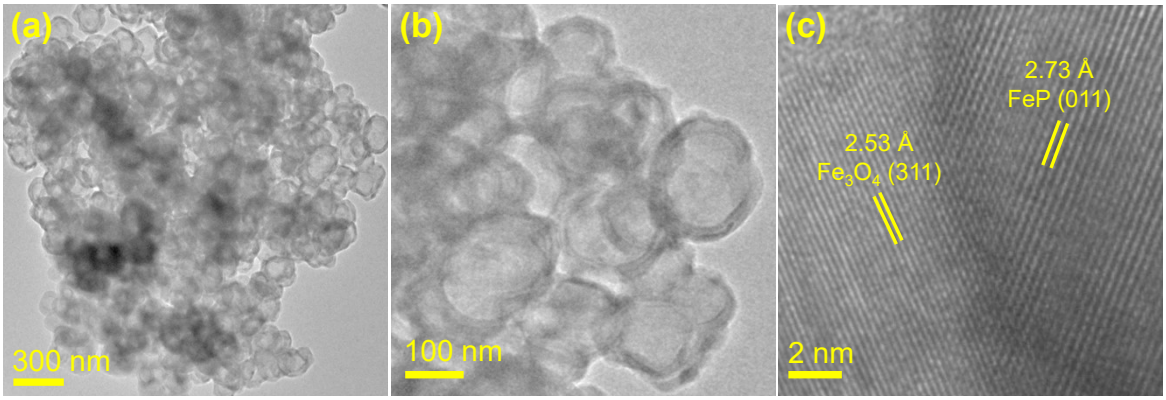

Fig. S8 TEM (a and b) and HR-TEM (c) of the FeP/Fe_3O_4/C obtained after durability test in 0.5 M H_2SO_4.

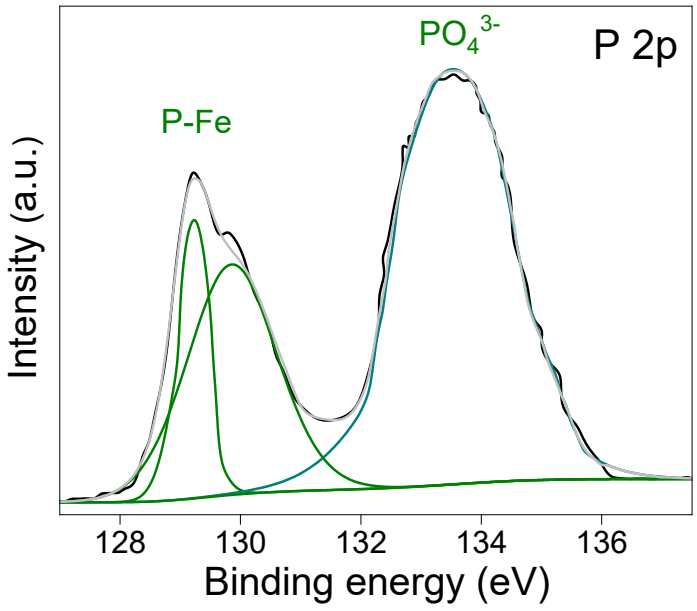

Fig. S9 XPS signatures of the FeP/Fe_3O_4/C obtained after durability test in 0.5 M H_2SO_4.

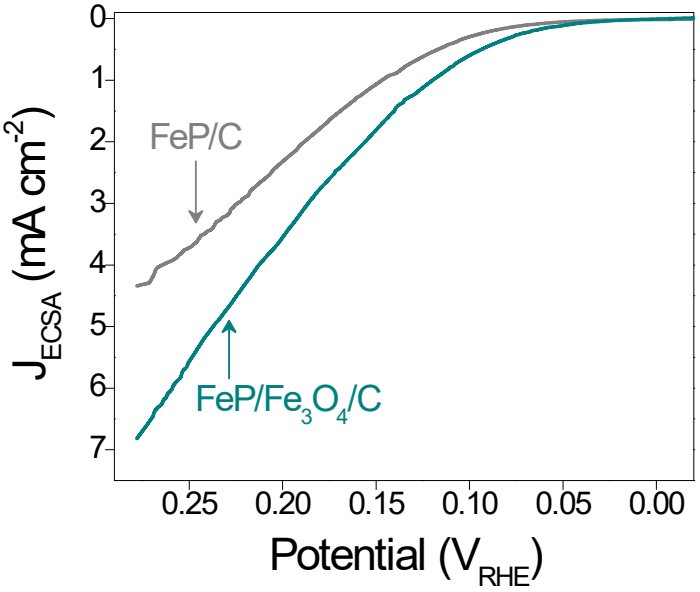

Fig. S10 Specific HER performance of FeP/C and FeP/Fe_3O_4/C under acidic medium.

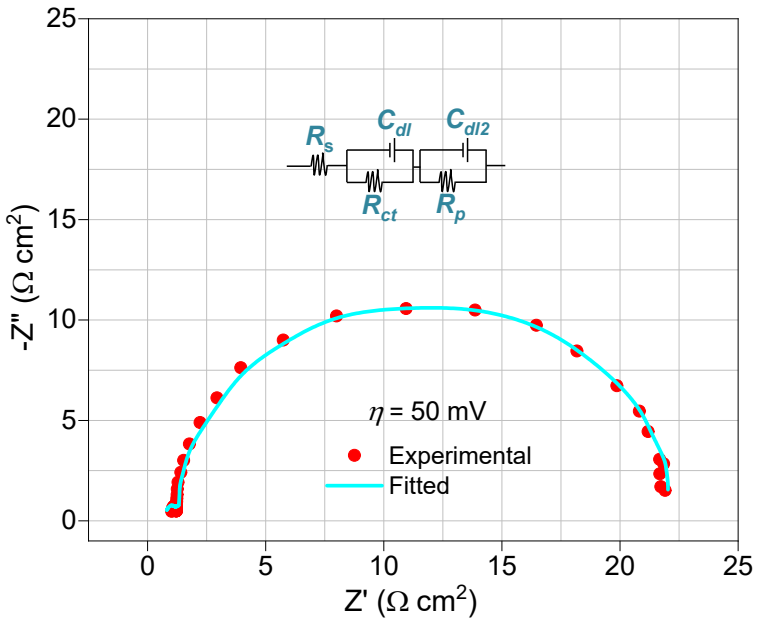

Fig. S11. Nyquist plots of the FeP/Fe_3O_4/C recorded at η = 50 mV showing experimental and fitted EIS results. Figure inset: Two time constant electrical equivalent circuit model utilized to fit the EIS data. R_s – series resistance, C_{dl} and C_{dl2} are double layer capacitance, R_{ct} – charge transfer resistance, R_p – resistance related to the surface porosity.

Table S1. Electrochemical impedance parameters of FeP/Fe_3O_4/C obtained by fitting the Nyquist plots to the equivalent circuit model (Figure inset).

Overpotential (mV)	R_s **(Ω)**	R_p **(Ω)**	R_{ct} **(Ω)**
0	0.73	0.04	169.70
50	0.72	0.28	20.48
100	0.73	0.34	2.96
130	0.74	0.30	1.28

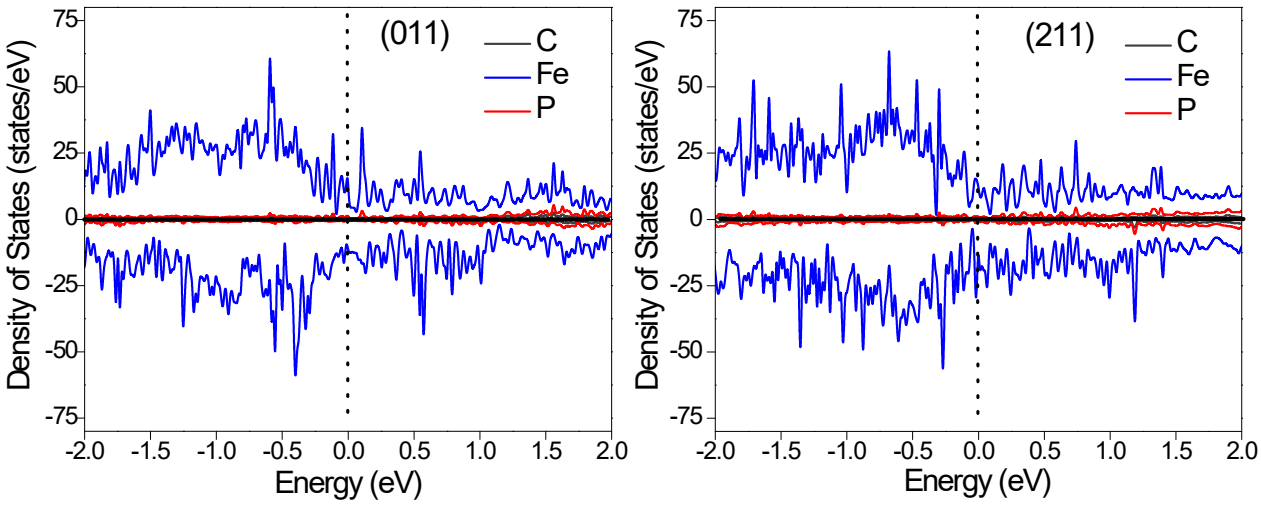

Fig. S12 Partial density of states of (011) and (211) surfaces in CFeP model. The Fermi level is set as zero and marked in dashed line.

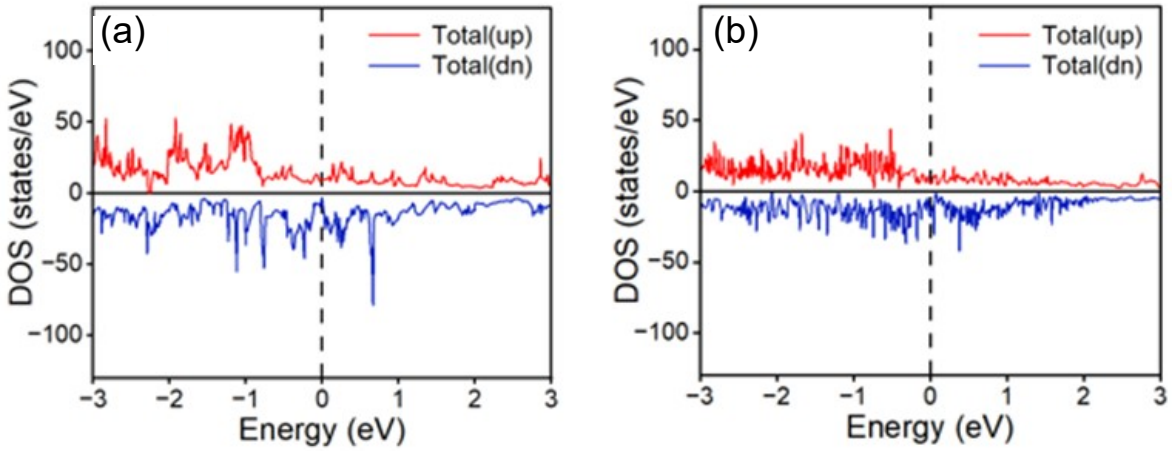

Fig. S13 Spin polarized density of electron state of FeP layer in (a) pristine FeP model and (b) FeP/Fe_3O_4 composite surface model. The Fermi level is set as zero and marked in dashed line.

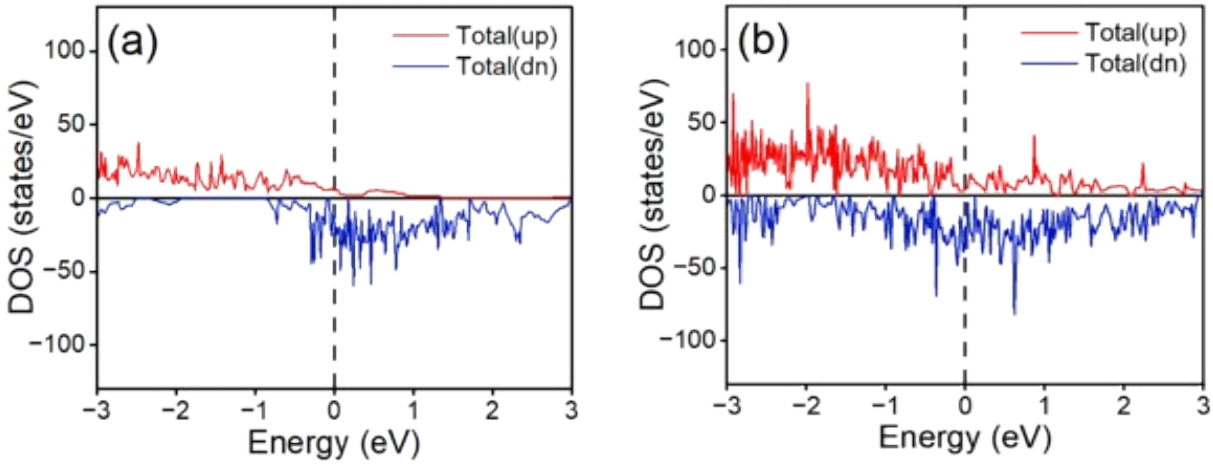

Fig. S14 Spin polarized DOS spectrums of two slab models. (a) Fe_3O_4 and (b) FeP-Fe_3O_4. The Fermi level is set as zero and marked with dashed line.

Table S2. Comparison of overpotential, Tafel slope and HER performance of electrocatalysts in acidic medium (0.5 M H_2SO_4).

Catalysts	Overpotential η_{10} (mV)	Tafel slope mV/dec	Catalyst loading (mg cm^{-2})
FeP/CN[S1]	104	63.5	1.00
FeP/C[S8]	71	52	0.44
FePNPs[S9]	154	65	0.90
Fe_2P @rGO[S10]	101	55	0.47
FeP NAs [S11]	58	45	1.50
Candle soot- FeP[S12]	112	58	0.28
FeP nanowires[S13]	96	39	60.0
Hollow FeP microspheres[S14]	144	58	0.27
Hollow FeP@C[S15]	115	56	NA
FeP Nanotubes/CF[S16]	88	36	1.60
FeP/G[S17]	123	50	0.28
FeP nanosheet[S18]	~240	67	~ 0.28
FeP mircospheres[S19]	66	53	0.56
Fe_2P/FG [S20]	91	47	0.40
FeP/C[S21]	157	127	0.40
FeP/carbon nanobox[S22]	119	53	~0.56
Hexagonal Fe_2P[S23]	214	107	NA
Orthorhombic Fe_2P [S23]	134	97	NA
Mn/FeP/C[S24]	143	58.4	~0.50
Fe/FeP/C[S25]	92	70.4	0.50
N-doped FeCoP[S26]	132	79	0.20
FeP NPs[S27]	153	115.5	2.0
3D FeP NR/PG[S27]	96	68.9	2.0
FeP/Fe_3O_4/C[This work]	90	62	1.00

C = Carbon; NPs = Nanoparticles; rGO = reduced graphene oxide; NAs = Nanorod Arrays; CN = Carbon Nanosheets; CF = Carbon fiber; FG = Fluffy Graphene, NR = Nanorods, PG = Phosphorous-doped graphene.

References

S1 M. H. Suliman, A. Adam, M. N. Siddiqui, Z. H. Yamani and M. Qamar, *Carbon*, 2019, **144**, 764-771.

S2 G. Kresse, D. Joubert, *Phys. Rev. B Condens. Matter*, 1999, **59**, 1758.

S3 H. Peng, J.P. Perdew, *Phys. Rev. B Condens. Matter*, 2017, **95**, 081105.

S4 H. J. Monkhorst, J.D. Pack, *Phys. Rev. B Condens. Matter*, 1976, **13**, 5188.

S5 S. Grimme, J. Antony, S. Ehrlich, H. Krieg, *J. Chem. Phys.*, 2010, **132**, 154104.

S6 J. K. Nørskov, T. Bligaard, A. Logadottir, J. R. Kitchin, J. G. Chen, S. Pandelov and U. Stimming, *J. Electrochem. Soc.*, 2005, **152**, J23–J26.

S7 W. Tang, E. Sanville and G. Henkelman, *J. Phys. Condens. Matter*, 2009, **21**, 084204.

S8 D. Y. Chung, S. W. Jun, G. Yoon, H. Kim, J. M. Yoo, K.-S. Lee, T. Kim, H. Shin, A. K. Sinha, S. G. Kwon, K. Kang, T. Hyeon and Y.-E. Sung, *J. Am. Chem. Soc*., 2017, **139**, 6669-6674.

S9 L. Tian, X. Yan, and X. Chen, *ACS Catal.,* 2016, **5**, 5441-5448.

S10 M. Liu, L. Yang, T. Liu, Y. Tang, S. Luo, C. Liu and Y. Zeng, *J. Mater. Chem. A*, 2017, **5**, 8608-15.

S11 Y. Liang, Q. Liu, A. M. Asiri, X. Sun and Y. Luo, *ACS Catal*., 2014, **7**, 4065-4069.

S12 Z. Zhang, J. Hao, W. Yang, B. Lu and J. Tang, *Nanoscale*, 2015, **7**, 4400-4405.

S13 C. Y. Son, I. H. Kwak, Y. R. Lim and J. Park, *Chem. Commun*., 2016, **52**, 2819-2822.

S14 X. Guo, Z. Feng, Z. Lv, Y. Bu, Q. Liu, L. Zhao, C. Hao, G. Li and Q. Lei, *ChemElectroChem*, 2017, **4**, 2052-2058.

S15 X. Zhu, M. Liu, Y. Liu, R. Chen, Z. Nie, J. Li and S. Yao, *J. Mater. Chem. A*, 2016, **4**, 8974-8977.

S16 Y. Yan, B. Y. Xia, X. Ge, Z. Liu, A. Fisher and X. Wang, *Chem. Eur. J.*, 2015, **21**, 18062-18067.

S17 Z. Zhang, B. Lu, J. Hao, W. Yang and J. Tang, *Chem. Comm*., 2014, **50**, 11554-11557.

S18 Y. Xu, R. Wu, J. Zhang, Y. Shi and B. Zhang, *Chem. Comm*., 2013, **49**, 6656-6658.

S19 C. Lin, Z. Gao, J. Yang, B. Liu and J. Jin, *J. Mater. Chem. A*, 2018, **6**, 6387-92.

S20 H. Huang, C. Yu, J. Yang, X. Han, C. Zhao, S. Li, Z. Liu and J. Qiu, *J. Mater. Chem. A*, 2016, **4**, 16028-16035.

S21 X.F. Lu, L. Yu, X. Wen(David) Lou, *Sci. Adv.*, 2019, **5**, eaav6009.

S22 Z. Peng, X. Qiu, Y. Yu, D. Jiang, H. Wang, G. Cai, X. Zhang and Z. Dong, *Carbon*, 2019, **152**, 16-23.

S23 S. Kong, P. Singh, A. Sarkar, G. Viswanathan, Y.V. Kolen'ko, Y. Mudryk, D.D. Johnson, and Kirill Kovnir, *Chem. Mater.,* 2024, **36**, 1665–1677.

S24 E. Soltani, M.B. Gholivand, M. Amiri, *Int. J. Hydrogen Energy*, 2024, **51**, 269–280.

S25 Q. Wang, Z. Fei, D. Shen, C. Cheng, P. J. Dyson, *Small*, 2023, 2309830.

S26 Z. Liu, T. Zhang, Y. Lin, H. Jia, Y. Wang, Y. Wang, G. Zhang, *Small*, 2023, **19**, 2302475.

S27 C. Yu, Y. Shi, F. Yan, Y. Zhao, C. Zhu, X. Zhang, X. Zhang, Y. Chen, *Chem. Eng. J.*, 2021, **423**, 130240.